

The Geometric Reasoner: Manifold-Informed Latent Foresight Search for Long-Context Reasoning

Ren Zhuang Ben Wang Shuifa Sun

Abstract

Scaling test-time compute enhances long chain-of-thought (CoT) reasoning, yet existing approaches face a fundamental trade-off between computational cost and coverage quality: either incurring high training expense or yielding redundant trajectories. We introduce The Geometric Reasoner (TGR), a training-free framework that performs manifold-informed latent foresight search under strict memory bounds. At each chunk boundary, TGR scores candidate latent anchors via a lightweight look-ahead estimate combined with soft geometric regularizers that encourage smooth trajectories and diverse exploration. Chunk-wise KV cache resets keep memory linear in chunk length. On challenging math and code benchmarks, TGR improves robust trajectory coverage, measured by the area under the Pass@ k curve (AUC), by up to 13 points on Qwen3-8B, with negligible overhead of about 1.1–1.3 \times .

1. Introduction

Scaling test-time compute reliably enhances large language model (LLM) performance, unlocking reasoning capabilities previously out of reach (Xu et al., 2025; Muenninghoff et al., 2025; Zhang et al., 2025b; Wu et al., 2025). Yet turning extra compute into diverse exploration without incurring prohibitive memory costs or wasting budget on redundant, correlated trajectories remains difficult. The quadratic complexity of attention and the footprint of KV caching (Vaswani et al., 2017; Beltagy et al., 2020; Dao et al., 2022; Dao, 2023) bottleneck practical deployment, rendering naive long-horizon exploration intractable.

Existing approaches make progress on this tension, yet critical gaps persist. Reinforcement Learning (RL) and preference optimization amortize long-horizon control into model weights (Schulman et al., 2017; Christiano et al., 2017; Shao

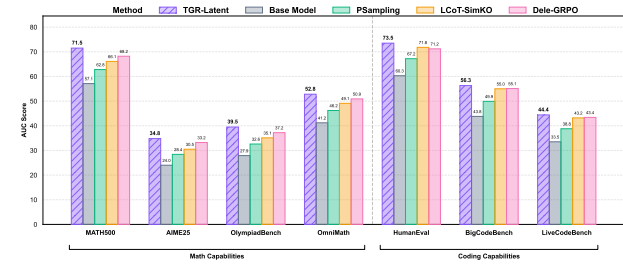


Figure 1. TGR-Latent consistently outperforms baselines on Qwen3-8B. Manifold-informed latent foresight search steering converts modest inference-time compute into robust coverage without weight updates.

et al., 2024; Zheng et al., 2025). While effective for single-sample accuracy, these methods demand substantial training compute and can collapse the trajectory distribution (Yue et al., 2025; Srivastava & Aggarwal, 2025). Sampling-based inference trades compute for robust coverage without re-training (Wang et al., 2022; Karan & Du, 2025; Faria et al., 2024), yet returns diminish rapidly as additional samples often remain correlated and fail to expand the set of distinct, valid trajectories (Tang et al., 2025; Wu et al., 2025). These limitations motivate a training-free inference-time search procedure that allocates compute dynamically under strict memory bounds.

To address this, we introduce **The Geometric Reasoner (TGR)**, a training-free framework for manifold-informed latent foresight search. TGR formulates reasoning as path search on a latent manifold but avoids rigid constraints that become brittle in high dimensions (Yallup et al., 2025; Be-tancourt, 2017; Goyal & Shetty, 2019). Instead, it ranks candidate reasoning chunks via a soft geometric score combining lightweight look-ahead utility, a bumpiness penalty for smooth transitions, and a repulsive diversity force that discourages similarity. Chunk-wise KV cache resets keep memory linear in chunk length, enabling scalable long-context exploration.

This chunk-boundary state interface relates to markovian control approaches that learn explicit state transitions, like

Delethink (Aghajohari et al., 2025). Rather than relying on learned state transitions or external verifiers, TGR enables training-free inference-time search, allocating compute to achieve controllable exploration and robust coverage under matched budgets.

Our contributions are:

- **Manifold-Informed Latent Foresight Search.** We propose TGR, a training-free inference-time framework that scores chunk-level latent anchors with a soft geometric objective, enabling controllable exploration without parameter updates.
- **Budget-Efficient Robustness.** TGR improves robust trajectory coverage on challenging math and code benchmarks, achieving up to 13-point AUC (area under the Pass@ k curve) gains on Qwen3-8B with negligible overhead of about 1.1–1.3 \times , as shown in Figure 1.
- **Scaling Limits of Hard Geometry.** We demonstrate that hard geometric filtering suffers from vanishing feasibility in high-dimensional latent spaces, where the acceptance rate decays exponentially as dimension increases, establishing soft geometric regularization as a scalable alternative.

2. Related Work

2.1. Test-time Reasoning

Prompt engineering steers model behavior via input formatting and exemplars, spanning in-context learning (Brown et al., 2020), Chain-of-Thought decomposition (Wei et al., 2022; Kojima et al., 2022), and program-aided methods such as PAL (Gao et al., 2023). These approaches improve controllability without additional training but remain sensitive to prompt design and operate via token-level heuristics.

Sampling-based reasoning includes local decoding controls (temperature, top- k , top- p), candidate pooling with Best-of- N selection (Wan et al., 2025), and aggregation methods such as Self-Consistency (Wang et al., 2022). Aggressive test-time sampling shows that additional inference compute can elicit latent reasoning without retraining (Karan & Du, 2025). Approaches such as Tree of Thoughts (ToT) (Yao et al., 2023) and Graph of Thoughts (GoT) (Besta et al., 2024) exemplify structured inference, which introduces explicit search in token space and trades computation for robustness. However, these methods search over discrete continuations and rely on token-space proxies or external scoring, rendering long-horizon search brittle under limited budgets.

2.2. Reinforcement Learning and Preference Optimization

Amortizing long-horizon control into model parameters via reinforcement learning and preference optimization has become a dominant paradigm (Christiano et al., 2017; Zhang et al., 2025a; Wiering & Van Otterlo, 2012). Beyond PPO (Schulman et al., 2017) and DPO (Rafailov et al., 2023), recent methods including GRPO (Shao et al., 2024) and GSPO (Zheng et al., 2025) scale reasoning by reducing reliance on a learned critic. Delethink (Aghajohari et al., 2025) learns discrete state transitions, demonstrating the utility of explicit Markovian states for long-horizon control. While effective, reward-and-preference-driven training exhibits failure modes at reduced diversity and overconfident generations (Yue et al., 2025; Srivastava & Aggarwal, 2025). SimKO (Peng et al., 2025) mitigates mode collapse and length bias, yet these training-centric approaches remain computationally intensive.

2.3. Geometric Perspectives on Latent Modeling

Geometric Deep Learning interprets learned representations as structured spaces (Bronstein et al., 2017; Higgins et al., 2017). Recent works frame attention as a geometric object governing representation transport along a curved manifold, treating layers as discrete geodesic steps shaped by training (Aggarwal et al., 2025; Di Sipio et al., 2025; Zhu et al., 2025). Complementing this view, LLM decoding is interpreted as tracing trajectories on a low-dimensional manifold, where coherent generations follow smooth paths and hallucinations appear as abrupt jumps (Zhang & Dong, 2025). These insights motivate geometric inductive biases at training time: manifold priors (Kang et al., 2025) and architectural constraints such as mHC (Xie et al., 2025), which applies Sinkhorn–Knopp normalization (Sinkhorn & Knopp, 1967) to confine signal propagation to a stable low-dimensional structure. Soft enforcement of geometry is preferred over hard feasibility filtering, which becomes impractical in high dimensions due to concentration of measure (Yallup et al., 2025; Betancourt, 2017; Goyal & Shetty, 2019). TGR operationalizes this insight at inference time, translating geometric priors into differentiable soft penalties without architectural changes.

Figure 2 contrasts TGR with test-time reasoning and RL methods, highlighting its training-free, manifold-informed latent foresight search.

3. Method

TGR is a training-free geometric reasoner that operates in latent space. It keeps the backbone LLM frozen, segments reasoning into chunks, and performs search at chunk boundaries within a continuous anchor space. At each boundary,

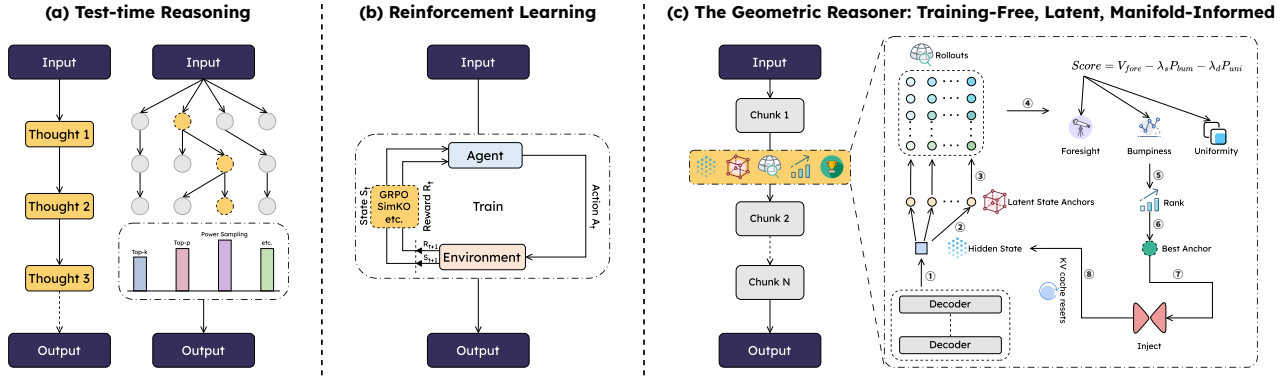


Figure 2. Overview of reasoning frameworks. Unlike (a) **test-time sampling**, exploring trajectories without explicit structure, or (b) **reinforcement learning**, which internalizes preferences through costly training, (c) TGR introduces a training-free inference-time search over the latent manifold. It selects optimal chunk-level anchors via a soft geometric score combining foresight, bumpiness, and uniformity, then injects them into generation with KV cache resets to maintain linear memory cost.

TGR samples candidate anchors, scores them using computationally efficient rollouts and soft geometric penalties, and selects the highest-scoring anchor to steer the subsequent chunk. Note that in this work, TGR denotes the latent-space variant TGR-Latent, unless explicitly stated otherwise.

3.1. Latent Space State Representation

Given a query Q , TGR generates output as a sequence of L chunks $\tau_{1:L} = (\tau_1, \dots, \tau_L)$, each of maximum length S . Let c_{t-1} denote the token context preceding chunk t . To bound memory during long-horizon decoding, we employ chunk-wise KV cache resets: at each boundary, we rebuild the prefix cache from c_{t-1} , discarding earlier history while transmitting long-range state via latent anchors (Appendix ??). Concretely, c_{t-1} comprises the query and recent token suffix, left-truncated to maximum length S .

3.1.1. STATE ANCHORS

We represent chunk-level reasoning states as unit-norm latent anchors on $\mathcal{Z} \triangleq \{x \in \mathbb{R}^{d_z} : \|x\|_2 = 1\}$. A state anchor $z_t \in \mathcal{Z}$ is extracted upon completing chunk t , serving as a compact chunk-boundary summary. Unlike Delethink (Aghajohari et al., 2025), which learns discrete state transitions, TGR extracts anchors directly from hidden states and performs score-guided anchor selection at inference time. This provides a summary for control under bounded KV cache constraints. At the next boundary, we sample K candidate anchors $\{\hat{z}_t^{(j)}\}_{j=1}^K \subset \mathcal{Z}$ centered at z_{t-1} , evaluate each via lightweight rollouts, and select the highest-scoring candidate to steer the next chunk.

This design addresses two inference constraints: chunk-wise KV resets require explicit state summaries for long-horizon coherence, and effective compute allocation demands a stateful interface rather than unstructured sampling.

3.1.2. STATE EXTRACTION

Upon generating τ_t , we append a fixed end-of-chunk delimiter token $\langle \text{EOC} \rangle$ and project its top-layer hidden state $h_{\text{eoc}}(\tau_t) \in \mathbb{R}^{d_h}$ onto the unit sphere, equivalently, the last hidden state of $\tau_t \oplus \langle \text{EOC} \rangle$:

$$z_t \triangleq \frac{W h_{\text{eoc}}(\tau_t)}{\|W h_{\text{eoc}}(\tau_t)\|_2} \in \mathcal{Z}, \quad (1)$$

where $W \in \mathbb{R}^{d_z \times d_h}$ is a fixed projection matrix. This yields a compact, model-internal summary facilitating chunk-to-chunk state transfer despite context truncation.

3.2. Foresight Search

We generate candidate anchors by sampling from the local neighborhood of the current state anchor via tangent-space perturbation followed by re-normalization:

$$\begin{aligned} \epsilon &\sim \mathcal{N}(0, I), \\ v &\leftarrow \epsilon - (z^\top \epsilon) z, \\ \tilde{a} &\leftarrow z + \sigma v, \\ a &\leftarrow \frac{\tilde{a}}{\|\tilde{a}\|_2} \in \mathcal{Z}, \end{aligned} \quad (2)$$

where z is the center anchor, setting $z = z_{t-1}$, and σ controls the exploration radius. Tangent-space perturbations preserve the local neighborhood structure on the unit sphere, avoiding radial drift associated with ambient space rescaling. We sample K candidate anchors $\{\hat{z}_t^{(j)}\}_{j=1}^K$ around z_{t-1} using Eq. (2). Each candidate is evaluated using the manifold-informed soft geometric score (Section 3.3), and the optimal anchor is selected to generate the subsequent chunk.

3.3. Manifold-Informed Regularization

We operationalize soft geometry as manifold-informed regularization that exploits local structure to guide search, leveraging tangent neighborhoods and curvature proxies. Unlike hard feasibility filtering, our approach translates geometric priors into differentiable soft penalties.

At each boundary, we score a candidate anchor a given context c and previous anchor z by maximizing:

$$\begin{aligned} \text{Score}(a; c, z) &= V_{\text{fore}}(a; c) \\ &\quad - \lambda_b P_{\text{bum}}(a; c) - \lambda_u P_{\text{uni}}(a; z). \end{aligned} \quad (3)$$

Here, $\lambda_b, \lambda_u \geq 0$ balance capability, coherence, and exploration.

3.3.1. FORESIGHT VALUE.

We estimate look-ahead value via a low-depth rollout of $s \ll S$ tokens under $p_\theta(\cdot | c, a)$, where p_θ denotes the frozen base model conditioned on anchor a via residual injection:

$$V_{\text{fore}}(a; c) \triangleq \mathbb{E} \left[\frac{1}{s} \sum_{i=1}^s \log p_\theta(\hat{\tau}_i | \hat{\tau}_{<i}; c, a) \right], \quad (4)$$

$$\hat{\tau}_{1:s} \sim p_\theta(\cdot | c, a).$$

We approximate this expectation with a single Monte Carlo rollout per candidate. In this setting, V_{fore} becomes a single-sample average log-likelihood proxy sufficient for ranking. This direct measurement of consistency in low-cost rollouts enables ranking without external reward models or trained verifiers.

3.3.2. BUMPINESS PENALTY.

Let $\mathbf{g}_1, \dots, \mathbf{g}_s$ be the top-layer hidden states along the rollout. We penalize high-frequency variation in the latent trajectory via a discrete second-order difference:

$$P_{\text{bum}}(a; c) \triangleq \frac{1}{s-2} \sum_{i=2}^{s-1} \|\mathbf{g}_{i+1} - 2\mathbf{g}_i + \mathbf{g}_{i-1}\|_2^2. \quad (5)$$

This term discourages abrupt directional changes, functioning as an efficient proxy for cross-chunk coherence.

3.3.3. UNIFORMITY REGULARIZER.

Since $a, z \in \mathcal{Z}$ are normalized, their semantic similarity reduces to a dot product. We enforce uniformity through repulsive interactions via a hinge penalty with threshold $\delta \in [0, 1)$, thereby promoting diverse exploration:

$$P_{\text{uni}}(a; z) \triangleq \max\{0, a^\top z - \delta\}. \quad (6)$$

This penalizes minimal-drift updates only when similarity exceeds δ (default $\delta = 0.2$, see Appendix ??).

Algorithm 1 TGR Reasoning Process

Require: Query Q , chunk limit L , chunk length S , candidate anchors K , rollout length s .
Require: Proposal radius σ , weights λ_b, λ_u , threshold δ .
Require: Frozen base model parameters θ ; fixed projection W defined in Eq. 1; fixed injectors $\{A_\ell, B_\ell\}$ defined in Eq. 8.
Ensure: Output trajectory $\tau_{1:T}$.

- 1: Initialize context $c_0 \leftarrow \text{Window}(Q)$.
- 2: Run frozen model on c_0 , set $z_0 \leftarrow \text{Normalize}(W h_{\text{eoc}}(c_0))$ via Eq. 1.
- 3: **for** $t = 1, \dots, L$ **do**
- 4: Rebuild prefix KV cache for c_{t-1} via chunk-wise reset.
- 5: **for** $j = 1, \dots, K$ **do**
- 6: Sample candidate $\hat{z}_t^{(j)} \leftarrow \text{SAMPLEAROUND}(z_{t-1}, \sigma)$ using Eq. 2.
- 7: Roll out $\hat{\tau}_{1:s}^{(j)} \sim p_\theta(\cdot | c_{t-1}, \hat{z}_t^{(j)})$ for s steps, applying residual injection via Eq. 8.
- 8: Compute foresight value $V_{\text{fore}}(\hat{z}_t^{(j)}; c_{t-1})$ via Eq. 4.
- 9: Compute bumpiness $P_{\text{bum}}(\hat{z}_t^{(j)}; c_{t-1})$ via Eq. 5.
- 10: Compute uniformity $P_{\text{uni}}(\hat{z}_t^{(j)}; z_{t-1})$ via Eq. 6.
- 11: Score $\mathcal{S}^{(j)} \leftarrow V_{\text{fore}} - \lambda_b P_{\text{bum}} - \lambda_u P_{\text{uni}}$ using Eq. 3.
- 12: **end for**
- 13: Select $j^* \leftarrow \arg \max_j \mathcal{S}^{(j)}$; set $\hat{z}_t \leftarrow \hat{z}_t^{(j^*)}$.
- 14: Generate chunk $\tau_t \sim p_\theta(\cdot | c_{t-1}, \hat{z}_t)$, length $\leq S$, via injection as in Eq. 8.
- 15: Extract new anchor $z_t \leftarrow \text{Normalize}(W h_{\text{eoc}}(\tau_t))$ via Eq. 1.
- 16: Update context $c_t \leftarrow \text{Window}(Q \oplus \tau_t)$ resetting KV cache.
- 17: **if** stopping criterion met **then**
- 18: **break**
- 19: **end if**
- 20: **end for**
- 21: **return** $\tau_{1:T}$

3.4. Overall Process

Algorithm 1 details the TGR inference process. At each boundary, we sample K candidate anchors, compute the manifold-informed score using efficient rollouts, select the highest-scoring anchor, generate the next chunk, and update the state anchor. Formally, letting $\mathcal{A}_t \triangleq \{\hat{z}_t^{(j)}\}_{j=1}^K$ be the candidate set at step t , we select:

$$\hat{z}_t \triangleq \arg \max_{a \in \mathcal{A}_t} \text{Score}(a; c_{t-1}, z_{t-1}). \quad (7)$$

Anchor conditioning via residual injection We condition on anchor $a_t \in \mathcal{Z}$ using a fixed low-rank residual injection at each transformer layer ℓ :

$$\begin{aligned} \mathbf{h}_\ell &\leftarrow \mathbf{h}_\ell + B_\ell A_\ell a_t, \\ A_\ell &\in \mathbb{R}^{r \times d_z}, \quad B_\ell \in \mathbb{R}^{d_h \times r}, \quad r \ll d_h. \end{aligned} \quad (8)$$

This creates a lightweight control interface without parameter updates. We inject at every layer using identical interfaces for candidate evaluation and generation, with fixed random matrices of rank r (default $r = 8$) to maintain the training-free setting (Appendix ??).

3.5. Vanishing Acceptance of Hard Geometric Constraints

A standard method for imposing latent geometric structure is hard feasibility filtering—accepting candidates only if they satisfy constraints such as geodesic-following, curvature caps, or angular thresholds.

Let a denote a candidate sampled from proposal distribution $q(\cdot | z_{t-1})$ centered at z_{t-1} , and let $\mathcal{F}_t^{\text{geo}}$ be the feasible set induced by a hard constraint, namely a curvature-bounded geodesic-following rule. The feasibility acceptance rate, i.e., pure accept/reject excluding likelihood ratios, is:

$$\begin{aligned} \alpha &\triangleq \Pr_{a \sim q(\cdot | z_{t-1})} [a \in \mathcal{F}_t^{\text{geo}}] \\ &= \mathbb{E}_{a \sim q(\cdot | z_{t-1})} [\mathbb{I}\{a \in \mathcal{F}_t^{\text{geo}}\}]. \end{aligned} \quad (9)$$

The expected number of proposals required to obtain one feasible sample is $\mathbb{E}[N_{\text{prop}}] = 1/\alpha$. Maintaining a fixed number of feasible candidates, such as K candidates per step, therefore requires inflating the proposal budget by a factor of roughly $1/\alpha$.

Crucially, α collapses rapidly in high-dimensional latent spaces due to concentration of measure; feasible regions often occupy an exponentially small fraction of the local neighborhood as dimensionality increases (Betancourt, 2017; Goyal & Shetty, 2019; Yallup et al., 2025). Table ?? illustrates that hard filtering becomes computationally prohibitive as dimension increases.

This motivates our use of soft geometry via manifold-informed regularization. Rather than rejecting candidates outside $\mathcal{F}_t^{\text{geo}}$, TGR integrates geometric priors as differentiable penalties within the scoring objective. This approach preserves geometric bias while circumventing the prohibitive $1/\alpha$ cost penalty of hard feasibility filtering.

4. Experiments

4.1. Experimental Setup

Models We use Qwen3 (Yang et al., 2025) as the primary testbed and report main results for the 8B variant; additional scales, 1.7B, 4B and 14B, are deferred to Appendix ?? . To study the interaction with training stages, we also evaluate Phi-4-reasoning (SFT Pre-Training) and Phi-4-reasoning-plus (with RL Post-Training) (Abdin et al., 2025).

Baselines We compare against (i) *training-free test-time compute* baselines: the base model and Power Sampling (PSampling) (Karan & Du, 2025); (ii) *RL-tuned approaches* that internalize long-CoT behaviors, including LCoT(GRPO) (Guo et al., 2025) and LCoT(SimKO) (Peng et al., 2025); (iii) *RL with structured state transitions*, instantiated by Delethink (Aghajohari et al., 2025) combined

with GRPO or SimKO; and (iv) *token-space control ablations*, which mirrors strong test-time strategies like Self-Consistency (Wang et al., 2022), ToT (Yao et al., 2023) or GoT (Besta et al., 2024) that operate in token-space under the same chunked interface.

Benchmarks For mathematics, we use MATH500 (Hendrycks et al., 2021), AIME2025 (MAA, 2025), OmniMath (Gao et al., 2024), and OlympiadBench (He et al., 2024). For code generation, we use HumanEval (Chen, 2021), BigCodeBench (Zhuo et al., 2024), and LiveCodeBench (Jain et al., 2024).

Unified inference budget and metrics. We report Pass@ k for $k \in \mathcal{K}$ and the normalized area under the Pass@ k curve, namely AUC as robustness metrics, along with Avg. Tokens, defined as the average end-to-end tokens per problem required to produce k final trajectories (Appendix ??).

We define the normalized AUC on a log scale as

$$\text{AUC} \triangleq \frac{100}{\log_2 k_M - \log_2 k_0} \sum_{i=0}^{M-1} \left(\log_2 k_{i+1} - \log_2 k_i \right) \cdot \frac{\text{Pass}@k_{i+1} + \text{Pass}@k_i}{2}, \quad (10)$$

where $\mathcal{K} = \{k_0 < \dots < k_M\}$. For code benchmarks, Pass@ k is computed using the unbiased estimator of Chen (2021). For math benchmarks, Pass@ k is the empirical success rate that at least one of k samples is correct. We use temperature 0.6 and the default TGR sampling with $K = 8$ candidate anchors per chunk boundary, scored by rapid rollouts ($s = 32$ on math tasks and $s = 64$ on code tasks); full hyperparameters are listed in Appendix ?? . We set an upper bound of $L = 24$ chunks with maximum chunk length $S = 512$, while actual generation terminates early by standard stopping criteria; all reported costs are based on realized token consumption.

4.2. Main Results

We evaluate TGR on math and code benchmarks under matched inference budgets. TGR-Latent consistently improves robust trajectory coverage while remaining token-efficient, indicating higher effective sample efficiency than both training-free sampling and training-heavy RL baselines. The comparison with TGR-Token isolates the benefit of latent-space search beyond discrete token-level control.

Mathematical Reasoning Table 1 reports results on Qwen3-8B. TGR-Latent consistently improves robust coverage, with gains scaling at medium-to-large sampling budgets. This indicates effective conversion of samples into distinct solution trajectories. Moreover, TGR attains these

Table 1. Mathematical reasoning results on Qwen3-8B. TGR-Latent matches or exceeds the best baseline on AUC while consuming 18% fewer tokens, demonstrating that inference-time latent search achieves superior budget-efficiency without training updates.

Method	AIME25				OlympiadBench				OmniMath				Tokens
	@1	@32	@128	AUC	@1	@32	@128	AUC	@1	@32	@128	AUC	
Base Model	18.7	26.5	28.4	24.0	22.1	30.2	32.6	27.9	31.4	45.8	48.9	41.2	2.6
PSampling	23.8	30.1	32.1	28.4	27.4	34.5	36.8	32.6	38.7	49.8	52.3	46.2	6.0
LCoT-GRPO	26.5	27.8	28.5	27.5	30.1	31.8	32.5	31.5	41.8	48.0	49.8	46.2	8.5
LCoT-SimKO	27.5	31.5	33.0	30.5	31.8	36.0	38.0	35.1	43.5	51.5	54.0	49.1	8.6
Dele-GRPO	27.4	35.5	37.8	33.2	31.5	39.0	41.8	37.2	43.1	54.2	57.1	50.9	8.4
Dele-SimKO	28.4	37.0	39.5	34.8	32.5	40.8	43.8	38.8	44.6	56.1	59.2	52.8	8.5
TGR-Token	25.4	33.2	35.6	31.1	29.1	37.0	39.5	34.8	41.2	53.0	55.8	49.3	7.5
TGR-Latent	27.8	37.4	40.1	34.8	32.8	41.8	44.9	39.5	43.8	56.8	60.1	52.8	7.0

Table 2. Code generation results on Qwen3-8B. TGR-Latent achieves the highest AUC on all three benchmarks and leads at high k , where latent-space diversity enables exploration of multiple valid coding solutions.

Method	HumanEval				BigCodeBench				LiveCodeBench				Tokens
	@1	@32	@128	AUC	@1	@32	@128	AUC	@1	@32	@128	AUC	
Base Model	45.7	67.8	71.2	60.3	34.1	48.5	51.3	43.8	26.8	36.8	38.9	33.5	1.6
PSampling	52.8	74.5	77.8	67.2	40.8	54.2	57.2	49.9	32.4	42.1	44.1	38.8	3.6
LCoT-GRPO	55.0	76.8	79.5	69.5	43.5	57.5	60.2	52.8	35.5	44.5	46.8	41.5	6.0
LCoT-SimKO	56.2	79.2	82.0	71.8	44.8	60.1	62.8	55.0	36.5	46.5	48.8	43.2	6.0
Dele-GRPO	<u>56.4</u>	79.8	82.5	71.2	44.8	60.5	63.3	55.1	36.4	46.8	49.1	43.4	5.9
Dele-SimKO	57.1	80.5	83.5	73.2	<u>45.5</u>	61.3	64.1	<u>56.0</u>	37.2	47.5	49.8	44.1	5.8
TGR-Token	55.3	78.5	81.8	70.8	43.5	58.8	61.4	53.6	35.1	45.5	47.8	42.0	4.4
TGR-Latent	56.1	81.1	84.2	73.5	45.6	62.1	64.8	56.3	<u>36.8</u>	48.1	50.2	44.4	4.6

gains with token costs competitive with training-heavy RL baselines.

Code Generation Table 2 summarizes code generation results. TGR-Latent improves AUC consistently while maintaining comparable token cost. The advantage is pronounced on coding tasks, which often admit multiple correct solutions. Substantial gains at higher k values are achieved by TGR through effective exploration of diverse coding trajectories in latent space.

Ablation of Geometric Components. Table 3 isolates each score component. Removing look-ahead value V_{fore} yields the largest degradation, confirming that look-ahead guidance from limited-horizon look-ahead rollouts is the primary driver. Removing uniformity P_{uni} substantially reduces AUC, indicating that repulsion is essential for candidate pool diversity. Bumpiness P_{bum} stabilizes multi-chunk coherence. The gap between TGR-Latent and TGR-Token suggests that improvements stem from latent-space search, not merely chunking.

4.3. In-Depth Analysis of TGR on Qwen3-8B

To understand TGR’s geometric design and clarify the source of its cost-robustness advantage, we interpret how soft geometric scoring balances foresight, smoothness, and

Table 3. Component ablation on Qwen3-8B. Lightweight foresight is essential for performance, while bumpiness and uniformity regularizers provide complementary gains. Latent-space control consistently outperforms its discrete token-level counterpart.

Method	MATH500	AIME25	Avg. AUC	Δ
TGR-Latent	71.5	34.8	53.2	-
- w/o P_{uni}	67.2	31.0	49.1	- 7.6%
- w/o P_{bum}	69.1	31.7	50.9	- 4.2%
- w/o V_{fore}	61.3	26.1	43.7	- 17.8%
- random anchor	55.1	21.5	38.3	- 27.9%
TGR-Token	66.4	31.1	48.8	- 8.3%

diversity to sustain effective coverage under budget constraints.

Inference scaling on MATH500. Figure 3 (left) plots Pass@ k on MATH500. The critical signal is the marginal gain as k increases. TGR-Latent sustains larger improvements at medium-to-large k , consistent with higher candidate independence. The repulsive term minimizes overlap, ensuring additional samples translate into new trajectory modes. Value-based look-ahead sharpens boundary selection, converting rollout compute into sustained gains.

Cost-robustness frontier. Figure 3 (middle, right) summarizes the cost-robustness trade-off. Methods relying on

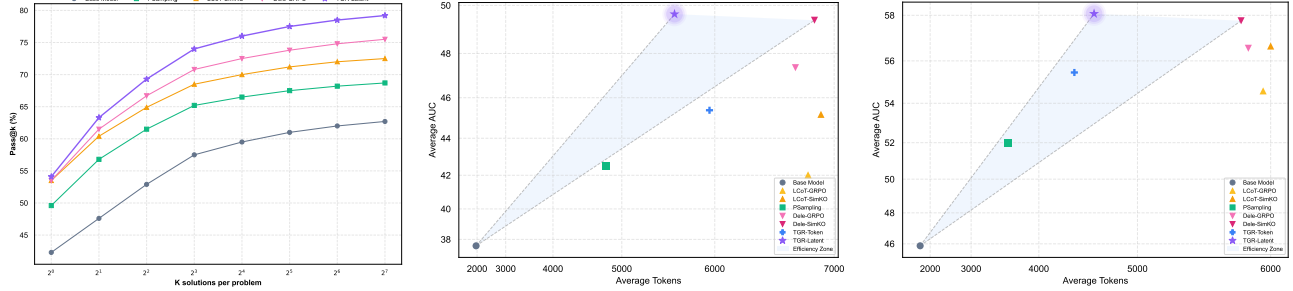


Figure 3. TGR dominates the inference efficiency frontier. **Left:** Pass@ k curves on MATH500 reveal that TGR-Latent sustains marginal gains beyond $k = 32$ where baselines plateau. **Middle & Right:** On the cost–robustness plane, TGR-Latent occupies the upper-left corner, achieving the highest AUC at moderate token cost on both math and code benchmarks.

training-heavy policies can incur substantial token cost without proportional coverage increase, while sampling-based approaches saturate early. TGR-Latent makes the most of its compute budget, allocating it to lightweight look-ahead and pruning low-yield exploration. This supports the conclusion that soft geometric scoring improves the conversion rate from inference compute to trajectory coverage.

Mode collapse and search dynamics. To diagnose diversity collapse, we analyze the geometry of within-step candidate anchors over time. As shown in Figure 4 (left), RL-tuned baselines concentrate probability mass in a narrow latent region, yielding highly correlated candidates and reduced coverage. In contrast, TGR maintains a dispersed anchor distribution, reflecting the effect of geometric repulsion in sustaining effective parallelism during scoring. This qualitative observation is quantified in Table ??, where removing P_{uni} collapses the candidate set toward a narrow cone, while the full model preserves meaningful separation.

Hyperparameter sensitivity. Figure 4 (right) reports sensitivity to rollout depth s and the candidate budget K , defined as the number of candidate anchors scored per boundary. Increasing either parameter improves AUC but with diminishing returns, while overhead grows approximately linearly. Consistent with the design goal of budget-aware inference-time search, where moderate look-ahead is sufficient to rank anchors reliably, and soft geometric penalties maintain diversity without excessive sampling, the default configuration lies near a stable operating region.

4.4. Interpreting TGR Representations

Beyond performance gains, we seek to interpret how TGR’s geometric design shapes its internal representations and search behavior, shedding light on the mechanisms underlying robust coverage.

Balancing Value, Bumpiness, and Uniformity in TGR. Soft geometric scoring manages a three-way trade-off

among look-ahead value, cross-chunk coherence, and exploration. Greedy decoding over-optimizes near-horizon likelihood; aggressive sampling sacrifices coherence. TGR makes this trade-off explicit via a single objective combining rollout value with bumpiness and uniformity regularizers. Regularization weights (λ_b, λ_u) control coherence and coverage. Empirically, removing V_{fore} degrades performance most, while removing P_{uni} primarily reduces AUC, indicating diminished parallelism.

Effective Independence Explains Stronger Gains in AUC than in Pass@1. AUC aggregates performance across the sampling scale, proxying the effective number of distinct trajectories. When candidates are correlated, increasing k yields diminishing returns. The uniformity term P_{uni} reduces overlap, ensuring additional compute translates into new solution modes. Thus, TGR’s advantage manifests primarily as higher AUC rather than Pass@1. Furthermore, Table ?? quantifies latent statistics showing that removing P_{uni} collapses effective candidate-set size N_{eff} .

Geometry–robustness diagnostics. We find that robustness exhibits a consistent geometric signature, with AUC peaking at an intermediate mean geodesic curvature κ that is neither overly rigid nor overly erratic and increasing with the effective candidate-set size proxy N_{eff} . This pattern supports the claim that TGR’s advantage stems from maintaining genuinely distinct search paths rather than redundant variations, as illustrated in Figure ??).

5. Discussion

5.1. Where Geometric Constraints Reside

Recent work interprets Transformer representations as trajectories on a latent manifold, with training objectives shaping its underlying geometry (Aggarwal et al., 2025; Di Sipio et al., 2025; Zhu et al., 2025; Xie et al., 2025). Building on this view, TGR operationalizes geometric structure at inference time through a manifold-informed scoring func-

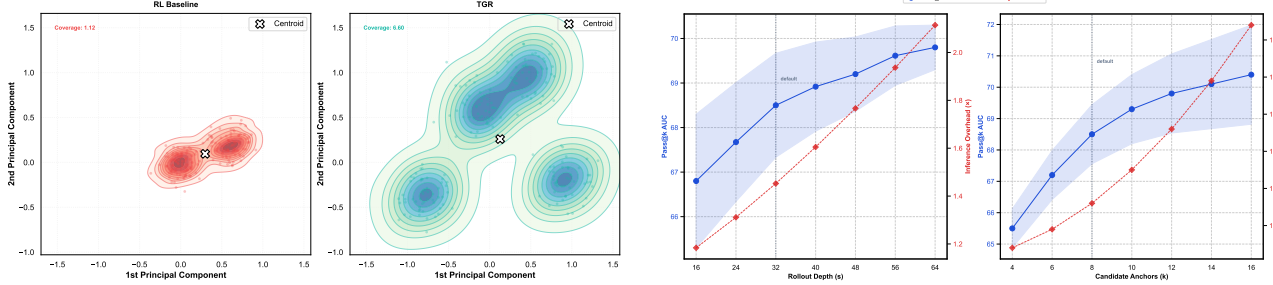


Figure 4. Left: Latent-space mode diversity. RL-tuned baselines collapse into a unimodal cone, while TGR preserves a well-dispersed distribution, capturing a fuller range of valid reasoning paths. **Right: Hyperparameter robustness.** AUC increases with rollout depth s and beam width K , but with diminishing returns.

tion over chunk-level candidates, enabling trajectory search without retraining. The key distinction lies in how geometric structure is instantiated. RL internalizes it into model weights, yielding strong single-trajectory priors but concentrating probability mass and limiting controllable exploration (Yue et al., 2025; Srivastava & Aggarwal, 2025). Training-time architectural regularization embeds it into the model parameterization, yet requires modifications to the training pipeline. In contrast, TGR externalizes geometric guidance as an inference-time control layer, offering tunable knobs that directly mediate the trade-off among look-ahead value, coherence, and diversity. This explicit control enhances robustness in long-horizon reasoning by increasing the effective independence of explored trajectories, naturally yielding higher AUC at medium-to-large sampling scales.

5.2. Training Stage Determines Inference-Time Controllability

This framing clarifies a key constraint on inference-time controllability, in which score guidance yields larger gains on SFT models than on heavily RL-optimized ones (Figure 5). Once training concentrates the trajectory distribution, degrees of freedom for inference-time search shrink; improvements manifest primarily as stabilizing coverage rather than shifting single-sample accuracy. Conversely, when training does not fully shape long-horizon behavior, explicit inference-time geometry provides a direct mechanism for allocating compute to high-yield branches while maintaining effective parallelism.

5.3. Limitations and Future Directions

TGR trades training cost for inference overhead, impacting latency-sensitive serving. Low-overhead rollouts serve as efficient proxies for downstream utility but may be less informative under delayed credit; adaptive budgeting or search at high-uncertainty boundaries offer mitigations.

Agentic workflows offer significant potential, yet failures frequently arise prior to tool execution due to unstable or

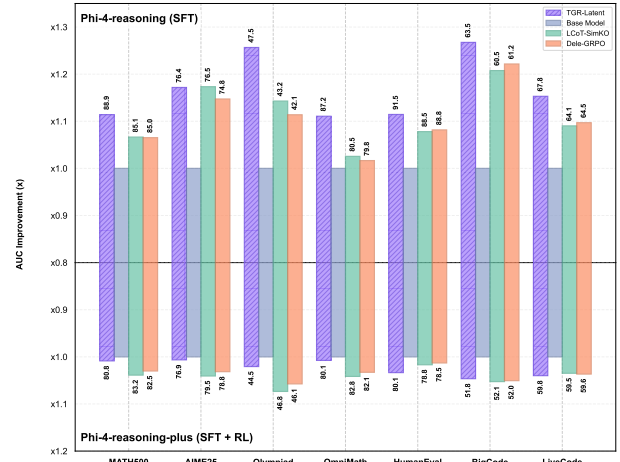


Figure 5. Training stage modulates inference-time controllability. TGR-Latent yields substantially larger gains on the SFT model (top), while improvement narrows after RL optimization (bottom), suggesting that inference-time search benefits models whose trajectory distribution retains residual flexibility.

ambiguous intent. A low-overhead latent foresight step guided by soft geometric principles could provide a reliable intent anchor prior to tool invocation, offering a potential mechanism to stabilize downstream planning.

6. Conclusion

We introduced TGR, a training-free inference-time framework that steers long-horizon reasoning via manifold-informed latent foresight search. By scoring chunk-level anchors with a soft geometric objective combining look-ahead value, coherence, and diversity penalties, TGR matches or exceeds RL-tuned baselines on challenging math and code benchmarks with negligible overhead. Decoupling lightweight boundary rollouts and geometric preferences from model training reveals that robust coverage need not be amortized through training but can instead be induced on the fly via structured latent-space search.

Impact Statement

This paper studies a training-free, manifold-informed latent foresight search framework for long-context reasoning. If effective, it may improve robustness under fixed or modestly increased compute budgets, benefiting applications such as programming assistance. As with other capability-improving methods, it could also enable misuse (e.g., harmful or misleading content) and its impact depends on deployment context. We recommend pairing such techniques with safeguards and careful evaluation before deployment.

References

Abdin, M., Agarwal, S., Awadallah, A., Balachandran, V., Behl, H., Chen, L., de Rosa, G., Gunasekar, S., Javaheripi, M., Joshi, N., et al. Phi-4-reasoning technical report. *arXiv preprint arXiv:2504.21318*, 2025.

Aggarwal, N., Dalal, S. R., and Misra, V. The bayesian geometry of transformer attention, 2025. URL <https://arxiv.org/abs/2512.22471>.

Aghajohari, M., Chitsaz, K., Kazemnejad, A., Chandar, S., Sordoni, A., Courville, A., and Reddy, S. The markovian thinker: Architecture-agnostic linear scaling of reasoning. *arXiv preprint arXiv:2510.06557*, 2025.

Beltagy, I., Peters, M. E., and Cohan, A. Longformer: The long-document transformer. *arXiv preprint arXiv:2004.05150*, 2020.

Besta, M., Blach, N., Kubicek, A., Gerstenberger, R., Podstawska, M., Gianinazzi, L., Gajda, J., Lehmann, T., Niewiadomski, H., Nyczk, P., et al. Graph of thoughts: Solving elaborate problems with large language models. In *Proceedings of the AAAI conference on artificial intelligence*, volume 38, pp. 17682–17690, 2024.

Betancourt, M. A conceptual introduction to hamiltonian monte carlo. *arXiv preprint arXiv:1701.02434*, 2017.

Bronstein, M. M., Bruna, J., LeCun, Y., Szlam, A., and Vandergheynst, P. Geometric deep learning: going beyond euclidean data. *IEEE Signal Processing Magazine*, 34(4): 18–42, 2017.

Brown, T., Mann, B., Ryder, N., Subbiah, M., Kaplan, J. D., Dhariwal, P., Neelakantan, A., Shyam, P., Sastry, G., Askell, A., et al. Language models are few-shot learners. *Advances in neural information processing systems*, 33: 1877–1901, 2020.

Chen, M. Evaluating large language models trained on code. *arXiv preprint arXiv:2107.03374*, 2021.

Christiano, P. F., Leike, J., Brown, T., Martic, M., Legg, S., and Amodei, D. Deep reinforcement learning from human preferences. *Advances in neural information processing systems*, 30, 2017.

Dao, T. Flashattention-2: Faster attention with better parallelism and work partitioning. *arXiv preprint arXiv:2307.08691*, 2023.

Dao, T., Fu, D., Ermon, S., Rudra, A., and Ré, C. Flashattention: Fast and memory-efficient exact attention with io-awareness. *Advances in neural information processing systems*, 35:16344–16359, 2022.

Di Sipio, R., Diaz-Rodriguez, J., and Serrano, L. The curved spacetime of transformer architectures. *arXiv preprint arXiv:2511.03060*, 2025.

Faria, G., Agrawal, S., Farinhas, A., Rei, R., de Souza, J., and Martins, A. Quest: Quality-aware metropolis-hastings sampling for machine translation. *Advances in Neural Information Processing Systems*, 37:89042–89068, 2024.

Gao, B., Song, F., Yang, Z., Cai, Z., Miao, Y., Dong, Q., Li, L., Ma, C., Chen, L., Xu, R., et al. Omni-math: A universal olympiad level mathematic benchmark for large language models. *arXiv preprint arXiv:2410.07985*, 2024.

Gao, L., Madaan, A., Zhou, S., Alon, U., Liu, P., Yang, Y., Callan, J., and Neubig, G. Pal: Program-aided language models. In *International Conference on Machine Learning*, pp. 10764–10799. PMLR, 2023.

Goyal, N. and Shetty, A. Sampling and optimization on convex sets in riemannian manifolds of non-negative curvature. In *Conference on Learning Theory*, pp. 1519–1561. PMLR, 2019.

Guo, D., Yang, D., Zhang, H., Song, J., Zhang, R., Xu, R., Zhu, Q., Ma, S., Wang, P., Bi, X., et al. Deepseek-r1: Incentivizing reasoning capability in llms via reinforcement learning. *arXiv preprint arXiv:2501.12948*, 2025.

He, C., Luo, R., Bai, Y., Hu, S., Thai, Z., Shen, J., Hu, J., Han, X., Huang, Y., Zhang, Y., et al. Olympiadbench: A challenging benchmark for promoting agi with olympiad-level bilingual multimodal scientific problems. In *Proceedings of the 62nd Annual Meeting of the Association for Computational Linguistics (Volume 1: Long Papers)*, pp. 3828–3850, 2024.

Hendrycks, D., Burns, C., Kadavath, S., Arora, A., Basart, S., Tang, E., Song, D., and Steinhardt, J. Measuring mathematical problem solving with the math dataset. *arXiv preprint arXiv:2103.03874*, 2021.

Higgins, I., Matthey, L., Pal, A., Burgess, C., Glorot, X., Botvinick, M., Mohamed, S., and Lerchner, A. betavae: Learning basic visual concepts with a constrained variational framework. In *International conference on learning representations*, 2017.

Jain, N., Han, K., Gu, A., Li, W.-D., Yan, F., Zhang, T., Wang, S., Solar-Lezama, A., Sen, K., and Stoica, I. Livecodebench: Holistic and contamination free evaluation of large language models for code. *arXiv preprint arXiv:2403.07974*, 2024.

Kang, H., Zhang, Y., Kuang, N. L., Majamaki, N., Jaitly, N., Ma, Y.-A., and Qin, L. Ladir: Latent diffusion enhances llms for text reasoning. *arXiv preprint arXiv:2510.04573*, 2025.

Karan, A. and Du, Y. Reasoning with sampling: Your base model is smarter than you think. *arXiv preprint arXiv:2510.14901*, 2025.

Kojima, T., Gu, S. S., Reid, M., Matsuo, Y., and Iwasawa, Y. Large language models are zero-shot reasoners. *Advances in neural information processing systems*, 35: 22199–22213, 2022.

MAA. American invitational mathematics examination - aime, 2025. URL <https://huggingface.co/datasets/math-ai/aime25>.

Muennighoff, N., Yang, Z., Shi, W., Li, X. L., Fei-Fei, L., Hajishirzi, H., Zettlemoyer, L., Liang, P., Candès, E., and Hashimoto, T. B. s1: Simple test-time scaling. In *Proceedings of the 2025 Conference on Empirical Methods in Natural Language Processing*, pp. 20286–20332, 2025.

Peng, R., Ren, Y., Yu, Z., Liu, W., and Wen, Y. Simko: Simple pass@ k policy optimization. *arXiv preprint arXiv:2510.14807*, 2025.

Rafailov, R., Sharma, A., Mitchell, E., Manning, C. D., Ermon, S., and Finn, C. Direct preference optimization: Your language model is secretly a reward model. *Advances in neural information processing systems*, 36: 53728–53741, 2023.

Schulman, J., Wolski, F., Dhariwal, P., Radford, A., and Klimov, O. Proximal policy optimization algorithms. *arXiv preprint arXiv:1707.06347*, 2017.

Shao, Z., Wang, P., Zhu, Q., Xu, R., Song, J., Bi, X., Zhang, H., Zhang, M., Li, Y., Wu, Y., et al. Deepseekmath: Pushing the limits of mathematical reasoning in open language models. *arXiv preprint arXiv:2402.03300*, 2024.

Sinkhorn, R. and Knopp, P. Concerning nonnegative matrices and doubly stochastic matrices. *Pacific Journal of Mathematics*, 21(2):343–348, 1967.

Srivastava, S. S. and Aggarwal, V. A technical survey of reinforcement learning techniques for large language models. *arXiv preprint arXiv:2507.04136*, 2025.

Tang, Y.-C., Chen, P.-Y., and Cavallaro, A. Carbon: Calibrated best-of-n sampling improves test-time reasoning. *arXiv preprint arXiv:2510.15674*, 2025.

Vaswani, A., Shazeer, N., Parmar, N., Uszkoreit, J., Jones, L., Gomez, A. N., Kaiser, Ł., and Polosukhin, I. Attention is all you need. *Advances in neural information processing systems*, 30, 2017.

Wan, G., Wu, Y., Chen, J., and Li, S. Reasoning aware self-consistency: Leveraging reasoning paths for efficient llm sampling. In *Proceedings of the 2025 Conference of the Nations of the Americas Chapter of the Association for Computational Linguistics: Human Language Technologies (Volume 1: Long Papers)*, pp. 3613–3635, 2025.

Wang, X., Wei, J., Schuurmans, D., Le, Q., Chi, E., Narang, S., Chowdhery, A., and Zhou, D. Self-consistency improves chain of thought reasoning in language models. *arXiv preprint arXiv:2203.11171*, 2022.

Wei, J., Wang, X., Schuurmans, D., Bosma, M., Xia, F., Chi, E., Le, Q. V., Zhou, D., et al. Chain-of-thought prompting elicits reasoning in large language models. *Advances in neural information processing systems*, 35:24824–24837, 2022.

Wiering, M. A. and Van Otterlo, M. Reinforcement learning. *Adaptation, learning, and optimization*, 12(3):729, 2012.

Wu, Y., Sun, Z., Li, S., Welleck, S., and Yang, Y. Inference scaling laws: An empirical analysis of compute-optimal inference for llm problem-solving. In *The Thirteenth International Conference on Learning Representations*, 2025.

Xie, Z., Wei, Y., Cao, H., Zhao, C., Deng, C., Li, J., Dai, D., Gao, H., Chang, J., Zhao, L., Zhou, S., Xu, Z., Zhang, Z., Zeng, W., Hu, S., Wang, Y., Yuan, J., Wang, L., and Liang, W. mhc: Manifold-constrained hyper-connections, 2025. URL <https://arxiv.org/abs/2512.24880>.

Xu, F., Hao, Q., Zong, Z., Wang, J., Zhang, Y., Wang, J., Lan, X., Gong, J., Ouyang, T., Meng, F., et al. Towards large reasoning models: A survey of reinforced reasoning with large language models. *arXiv preprint arXiv:2501.09686*, 2025.

Yallup, D., Kroupa, N., and Handley, W. Nested slice sampling. In *Frontiers in Probabilistic Inference: Learning meets Sampling*, 2025.

Yang, A., Li, A., Yang, B., Zhang, B., Hui, B., Zheng, B., Yu, B., Gao, C., Huang, C., Lv, C., et al. Qwen3 technical report. *arXiv preprint arXiv:2505.09388*, 2025.

Yao, S., Yu, D., Zhao, J., Shafran, I., Griffiths, T., Cao, Y., and Narasimhan, K. Tree of thoughts: Deliberate problem solving with large language models. *Advances in neural information processing systems*, 36:11809–11822, 2023.

Yue, Y., Chen, Z., Lu, R., Zhao, A., Wang, Z., Song, S., and Huang, G. Does reinforcement learning really incentivize reasoning capacity in llms beyond the base model? *arXiv preprint arXiv:2504.13837*, 2025.

Zhang, K., Zuo, Y., He, B., Sun, Y., Liu, R., Jiang, C., Fan, Y., Tian, K., Jia, G., Li, P., et al. A survey of reinforcement learning for large reasoning models. *arXiv preprint arXiv:2509.08827*, 2025a.

Zhang, Q., Lyu, F., Sun, Z., Wang, L., Zhang, W., Hua, W., Wu, H., Guo, Z., Wang, Y., Muenninghoff, N., et al. A survey on test-time scaling in large language models: What, how, where, and how well? *arXiv preprint arXiv:2503.24235*, 2025b.

Zhang, Y. and Dong, Q. Dynamic manifold evolution theory: Modeling and stability analysis of latent representations in large language models. *arXiv preprint arXiv:2505.20340*, 2025.

Zheng, C., Liu, S., Li, M., Chen, X.-H., Yu, B., Gao, C., Dang, K., Liu, Y., Men, R., Yang, A., et al. Group sequence policy optimization. *arXiv preprint arXiv:2507.18071*, 2025.

Zhu, H., Zhang, Z., Huang, H., Su, D., Liu, Z., Zhao, J., Fedorov, I., Pirsavash, H., Sha, Z., Lee, J., et al. The path not taken: Rlvr provably learns off the principals. *arXiv preprint arXiv:2511.08567*, 2025.

Zhuo, T. Y., Vu, M. C., Chim, J., Hu, H., Yu, W., Widyasari, R., Yusuf, I. N. B., Zhan, H., He, J., Paul, I., et al. Bigcodebench: Benchmarking code generation with diverse function calls and complex instructions. *arXiv preprint arXiv:2406.15877*, 2024.